Human Molecular Genetics, 2018, Vol. 27, No. 24 4169–4175

doi: 10.1093/hmg/ddy289
Advance Access Publication Date: 14 August 2018
General Article

GENERAL ARTICLE

A novel mouse model of hemangiopericytoma due to loss of Tsc2

Heng Du[1,†], John R. Dreier[1,†], Mahsa Zarei[1,2], Chin-Lee Wu[3], Roderick W. Bronson[4] and David J. Kwiatkowski[1,*]

[1]Division of Pulmonary Medicine, Department of Medicine, Brigham and Women's Hospital, Harvard Medical School, Boston, MA, 02115, USA, [2]Department of Veterinary Physiology and Pharmacology, Texas A & M University, College Station, TX, 77843, [3]Departments of Pathology and Urology, Massachusetts General Hospital, Harvard Medical School, Boston, MA, 02114, USA and [4]Department of Pathology, Harvard Medical School, Boston, MA, 02115, USA

*To whom correspondence should be addressed at: 20 Shattuck St., Thorn 826, Boston, MA, 02115, USA. Tel: 857 3070781; Fax: 857 3070780; Email: dk@rics.bwh.harvard.edu

Abstract

Hemangiopericytoma (HPC) is a rare vascular tumor, which is thought to originate from pericytes. However, no direct evidence for the cell of origin has been found, and the mechanism of HPC tumorigenesis is poorly understood. Here we report that loss of the tumor suppressor gene *Tsc2* in pericytes using a FoxD1 promoter driven cre allele (*Foxd1*$^{tm1(GFP/cre)\ Amc}$, *FoxD1*^{GC}) leads to the formation of HPC in multiple sites. *Tsc2*^{ff}*FoxD1*^{GC} mice had stunted growth with seizures and tail and hind limb tremor with a median survival of 110 days. They also showed recombination in brain, spinal cord, tongue, liver, intestine and skeletal muscle. Distinctive perivascular tumors consisting of cells with oval nuclei and scant cytoplasm were identified in multiple sites in all *Tsc2*^{ff}*FoxD1*^{GC} mice. Immunohistochemistry staining showed a high expression of phospho-S6-S240/244, a hallmark of activated mTORC1, as well as pericyte markers NG2 and vimentin in these tumors. In summary, we demonstrate that loss of *Tsc2* in pericytes generates HPC, the first mouse model of HPC reported.

Introduction

Hemangiopericytoma (HPC), a rare vascular tumor thought to originate from pericytes, was first defined by Stout and Murray in 1942 (1). HPC was originally classified into adult and infantile variants, but they are now thought to be different pathologic entities due to their different clinical manifestations and histomorphologies (2). Adult HPC has overlapping features with solitary fibrous tumors (SFT). However, infantile HPC is closely related to infantile myofibromatosis. Adult HPC occurs in middle-aged and older patients with an equal sex distribution, whereas infantile HPC occurs either congenitally or in the first few years of life (3,4). The pelvis and retroperitoneum are the most commonly involved organs in adult women (5). Furthermore, HPC commonly arises in the meninges, representing 2–4% of all meningeal tumors (6). Most HPC are benign, but 10–20% are of borderline or frank malignant potential as assessed by nuclear atypia, mitotic activity and clinical characteristics (7). Although the pericyte has been thought to be the cell of origin of HPC for many years, direct proof of this has been elusive.

Pericytes were first described in 1871 by Eberth (8). They are a population of vascular mural cells that surround the endothelial

[†]These authors contributed equally to this work.

Received: April 6, 2018. **Revised:** July 9, 2018. **Accepted:** August 6, 2018

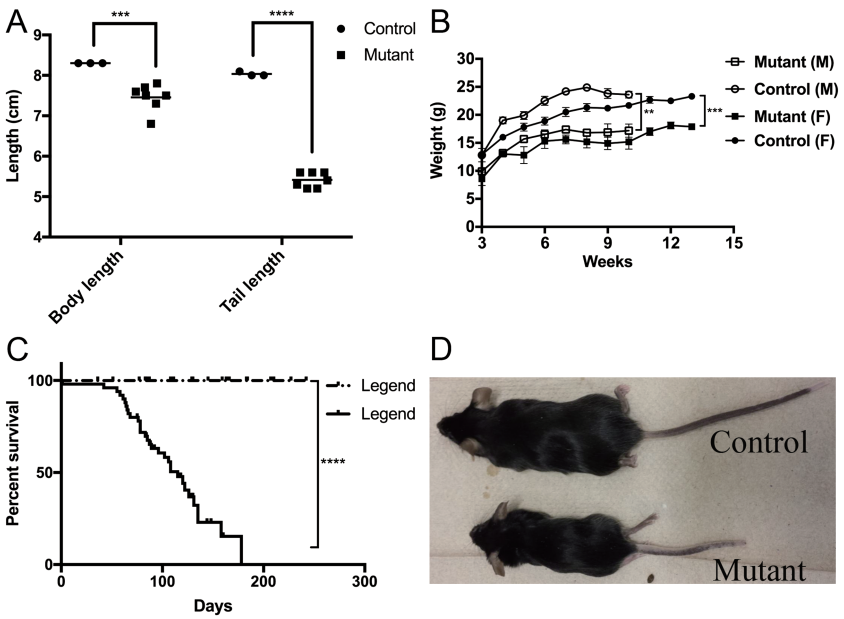

Figure 1. Growth retardation and early mortality in *Tsc2*^{ff} FoxD1 $^{GC+}$ mice. (A) *Tsc2*^{ff}*FoxD1*$^{GC+}$ (Mutant) mice have a shortened body and tail length in comparison to control littermates (***denotes $P < 0.001$, **** denotes $P < 0.0001$). **(B)** *Tsc2*^{ff}*FoxD1*$^{GC+}$ mice have a lower body weight than controls in both sexes (n = 14–34 for the 4 categories are shown). **(C)** Survival curve of *Tsc2*^{ff}*FoxD*$^{GC+}$ mice (n = 40; median, 115 days) compared to control littermates (n = 35). **(D)** Photograph of representative adult *Tsc2*^{ff}*FoxD1*$^{GC+}$ mouse (age, 6 months) in comparison to control littermate.

cells (ECs) of small blood vessels, being found below the smooth muscle cell (SMC) layer seen in larger vessels (9). Pericytes act as regulators of vascular morphogenesis during development and cardiovascular homeostasis (10). Pericytes also play roles in the development of diabetic retinopathy and tissue fibrosis (11,12). Some pericytes can give rise to adipocytes, cartilage, bone and muscle, such that some are thought to have mesenchymal stem or progenitor cell properties (10,13–16).

Tuberous Sclerosis Complex (TSC) is due to mutations in either the *TSC1* or *TSC2* tumor suppressor genes. TSC1 (hamartin) and TSC2 (tuberin) form a heterotrimeric complex, along with TBC1D7, which acts as a critical regulator of the mammalian target of rapamycin complex 1 (mTORC1) through its action on the RHEB GTPase (17). Genetic loss of both alleles of either *TSC1* or *TSC2* leads to constitutive activation of mTORC1, leading to unregulated synthesis of biosynthetic precursors including nucleotides, lipids and proteins, as well as macromolecular structures such as ribosomes, enlarged cell size and promotes tumor development (18–20). Several tumors and other lesions occurring in TSC individuals at high frequency are characterized by abnormal vascular structures, including renal angiomyolipoma and pulmonary lymphangioleiomyomatosis. Furthermore, previous studies have shown that the distinctive vessels of renal angiomyolipoma are neoplastic and positive for pS6 staining (21). In addition, renal angiomyolipoma have been shown to express pericyte antigens including α-smooth muscle actin (α-SMA), desmin, CD146 and platelet-derived growth factor receptor-β (PDGFR-β) (22,23), suggesting that renal angiomyolipoma may originate from pericytes (23).

Hence, we examined the possibility that loss of *Tsc2* in pericytes in the mouse might lead to vascular pathology similar to that seen in TSC. We found consistent HPC development in multiple organs in these mice, but no evidence of renal angiomyolipoma or lymphangioleiomyomatosis.

Results

Tsc2^{ff} *FoxD1*$^{GC+}$ mice display growth inhibition, seizures, focal weakness and early mortality

We targeted pericytes for selective loss of *Tsc2* using a cre allele in which cre expression is driven by the FoxD1 promoter, *FoxD1*^{GC} (24), combined with a floxed allele of *Tsc2*, *Tsc2*^{f} (25). A total of 40 *Tsc2*^{ff}*FoxD1*$^{GC+}$ and 35 control mice (*Tsc2*^{fw} *FoxD1*$^{GC+}$ *tdTomato*$^{+}$ and *Tsc2*^{ff} *FoxD1*$^{GC-}$ *tdTomato*$^{+}$) were generated from the same litters. *Tsc2*^{ff}*FoxD1*$^{GC+}$ mice had a significant reduction in both body length (7.46 ± 0.13 versus 8.30 ± 0.05 cm, $P = 0.00005$) and a drastically shortened tail length (5.41 ± 0.07 versus 8.03 ± 0.03, $P < 0.00001$) compared to control littermates (Fig. 1A and D). Both male and female *Tsc2*^{ff}*FoxD1*$^{GC+}$ mice showed significant differences in weight gain compared to controls ($P < 0.01$ and $P < 0.001$, respectively; Fig. 1B). In addition, *Tsc2*^{ff}*FoxD1*$^{GC+}$ mice showed a median survival of 115 days (Fig. 1C).

Tsc2^{ff}*FoxD1*$^{GC+}$ mice developed multifocal HPCs in different organs

Whole-mouse necropsy was performed on 8 *Tsc2*^{ff}*FoxD1*$^{GC+}$ mice at the age of 6 months, and multiple tumors were identified in the head (8 of 8), tongue (8 of 8) and tails (8 of 8). No tumors were seen in these regions in the control group that also had whole-mouse necropsy (n = 4). The tumors were somewhat variable but were typically well circumscribed and composed of cytologically uniform small, basophilic, ovoid to spindled cells with an oval nucleus and ill-defined cytoplasm. These cells were disorganized and surrounded numerous thin-walled ramifying blood vessels (Fig. 2 left column, H&E; Fig. S2A and D).

The tripartite organization of a canonical blood vessel includes ECs, SMCs and pericytes. We anticipated that the tumors seen were derived from pericytes, given the cre allele

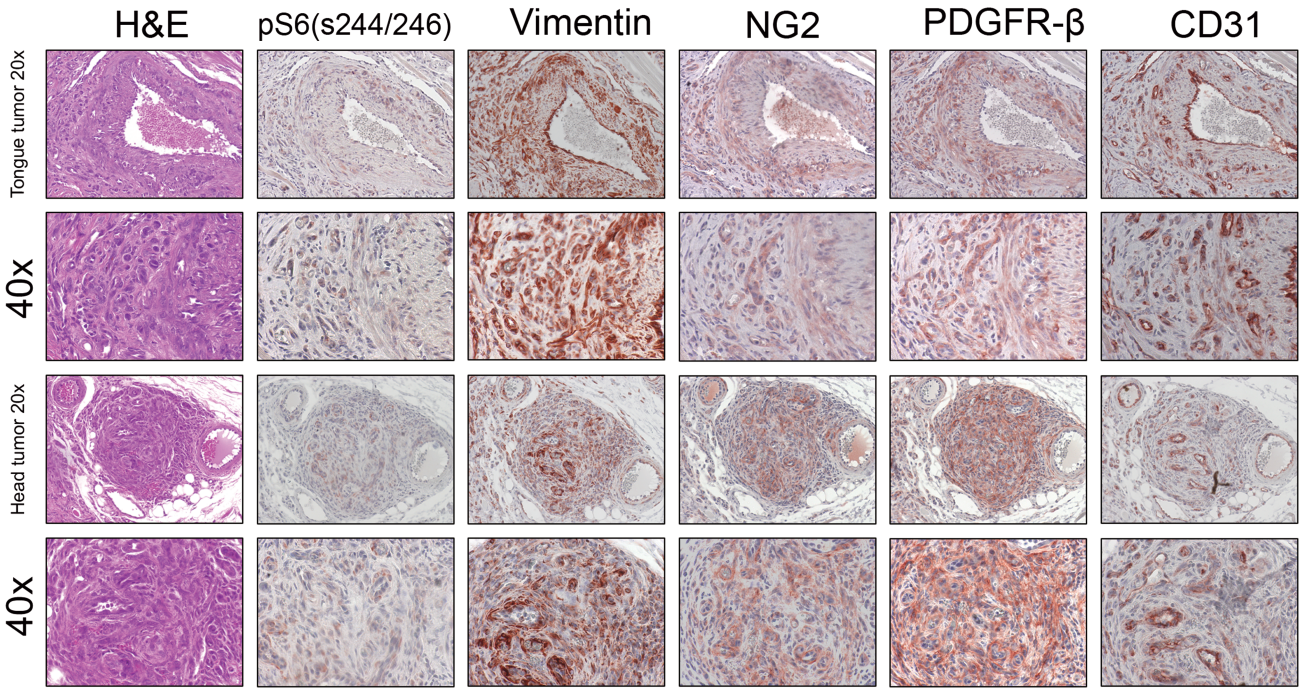

Figure 2. Multifocal HPC in the tongue and face of *Tsc2*^{ff} *FoxD1*$^{GC+}$ mice. H&E stains and IHC using serial sections for pS6 (S244/246), vimentin, NG2, PDGFR-β and CD31 are shown for two different HPC occurring in the tongue and face. Note pS6 (S244/246) expression by the pericyte tumor cells reflecting mTORC1 activation. Note the expression of typical markers (vimentin, NG2, PDGFR-β) of pericytes in the tumors, and of CD31 by ECs but not in tumor cells.

that had been used, and used cell type-specific markers to assess this by immunohistochemistry (IHC). All the tumors examined from multiple locations were strongly positive for vimentin, an intermediate filament protein commonly used as a pericyte marker, and showed diffuse staining of NG2 and PDGFR-β, both of which are also commonly used to label pericytes (Fig. 2). In contrast, aberrant small blood vessels within these tumors showed high expression of the EC marker CD31, which was not expressed by the tumor cells (Fig. 2 right column, CD31). Tongues from control mice did not show any tumors and only normal small blood vessels were highlighted by CD31 (Fig. S1). As noted above, most human HPCs are benign, and HPCs found in our mouse model showed no mitotic figures and were negative for each of Phospho-Histone H3 (Ser10) (Fig. S2B and E) and Ki67 staining (data not shown).

mTOR hyperactive pericytes induced by Tsc2 recombination contribute to multifocal HPCs

To assess the extent of *Tsc2* recombination, the *tdTomato* reporter allele was introduced, producing *Tsc2*^{ff}*FoxD1*$^{GC+}$ *tdTomato*$^{+}$ mice. Immunofluorescence (IF) on frozen sections revealed extensive recombination in pericytes in the tongue (Fig. 3A) and intestine (Fig. 3C), confirming that recombination in pericytes was occurring to cause tumor formation. Tongues from control mice (*Tsc2*^{ff} *FoxD1*$^{GC-}$ *tdTomato*$^{+}$) did not show red dTomato fluorescence indicative of a lack of recombination (Fig. 3B). None of the 8 *Tsc2*^{ff}*FoxD1*$^{GC+}$ mice subject to whole-mouse necropsy showed any significant pathology in the kidney or lung, even though pericytes in the kidney showed evidence of recombination in *Tsc2*^{ff} *FoxD1*$^{GC+}$ *tdTomato*$^{+}$ mice (n = 8; Fig. 3D, E, F). Pericytes in HPCs from both the tongue and face were positive for pS6 (S244/246) and vimentin, (Fig. 2, pS6 (S244/246); Fig. S2C and F), confirming that mTORC1 was activated secondary to Tsc2 loss in these cells.

Pathological and clinical effects of loss of *Tsc2* in other cell types

In addition to the expected recombination in pericytes, we saw evidence for recombination in other cell types in *Tsc2*^{ff}*FoxD1*$^{GC+}$ mice. Expansion of one or more vertebral bodies of *Tsc2*^{ff}*FoxD1*$^{GC+}$ mice caused some degree of cord compression in 6 of the 8 mice subject to whole-mouse necropsy (Fig. 4B), whereas the control mice (*Tsc2*^{fw}*FoxD1*$^{GC+}$) (Fig. 4A) had normal vertebral bodies. This was likely due to recombination and loss of Tsc2 in osteoblasts and/or osteoclasts, which is known to cause bone cortical hypertrophy (26). Neurons in both the spinal cord (Fig. 4D, E, F) and brain (data not shown) showed marked enlargement in comparison to controls (Fig. 4G, H, I) and were likely the cause of spontaneous seizures as well as tail and hind limb tremor in 6 of 8 of Tsc2ffFoxD1GC+ mice. Similar findings have been made previously in brain-specific models of TSC (27,28).

Discussion

HPC was first described in 1942, and has been a focus of pathologic investigation since then (1). The 2013 World Health Organization (WHO) classification of tumors of soft tissue and bone considers HPC and SFT to be synonyms for the same tumor type, which is currently called SFT within the category of fibroblastic/myofibroblastic tumors (29). The majority of SFTs occur in the pleura, meninges and soft tissue locations, and are rare in all sites (5,6). About 10% have an aggressive clinical behavior with local or distant recurrence. Surgical resection is the main treatment approach (7).

A major advance in our understanding of the pathogenesis of these rare tumors was the identification of recurrent gene fusions involving the genes *NAB2* and *STAT6* in SFT/HPC (30).

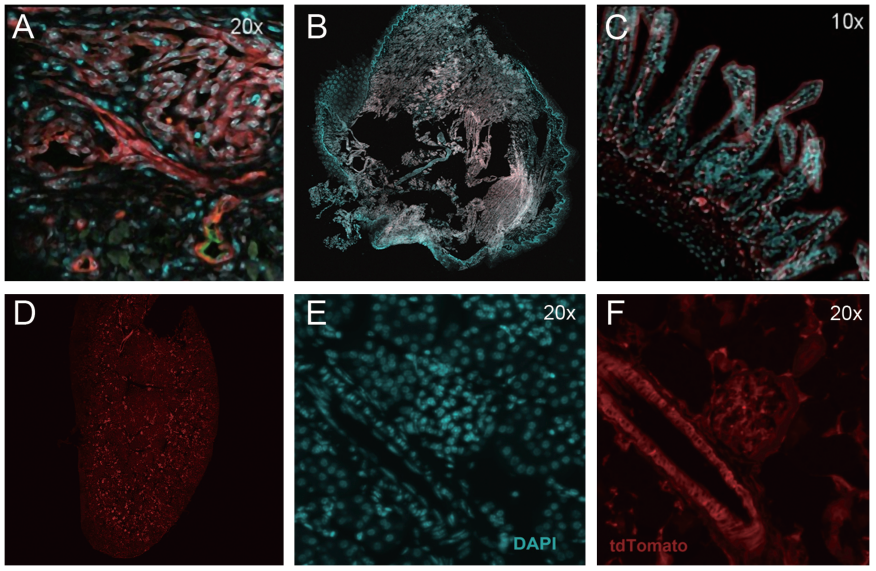

Figure 3. Recombination in pericytes in *Tsc2*^{ff} *FoxD1*$^{GC+}$ *tdTomato*$^{+}$ mice. Recombination, as assessed by tdTomato fluorescence, can be seen in a tongue HPC (**A**), intestinal wall pericytes (**C**) and pericytes from kidney blood vessels and glomeruli (**D–F**). Tongue from control mouse (**B**, *Tsc2*^{fw} *FoxD1*$^{GC+}$) showed no tdTomato fluorescence, indicating absence of recombination. Red reflects dTomato fluorescence (A, B, C, D, F), cyan indicates DAPI labeled nuclei (A, B, C, E), and the green counterstain in the tongue is endomucin (A, EC marker). Note that A-C are fused images, while D shows the whole image of kidney by tdTomato alone, E shows DAPI signal alone, and F tdTomato fluorescence alone.

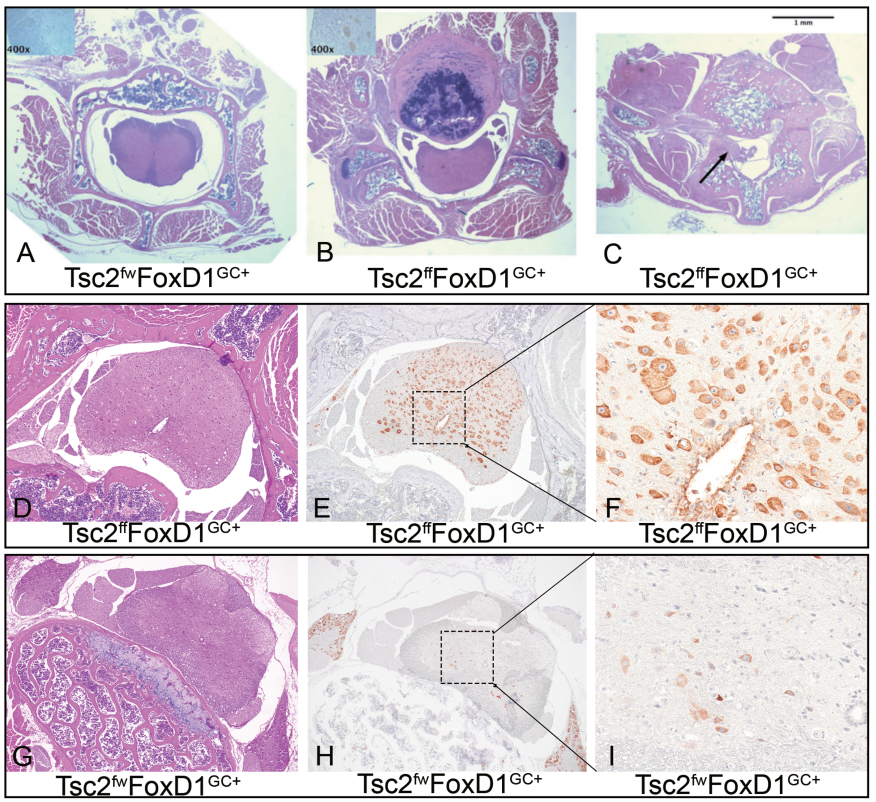

Figure 4. Spinal cord abnormalities in *Tsc2*^{ff} *FoxD1*$^{GC+}$ mice. (A-C) Low power magnification (2x) of spinal column cross-sections. (**A**) control genotype mouse, (**B**) hypertrophic vertebral body compressing the cord in *Tsc2*^{ff}*FoxD1*$^{GC+}$ mouse, (**C**) HPC invasion into the spinal canal (arrow) in a different *Tsc2*^{ff}*FoxD1*$^{GC+}$ mouse. (**D–F**) Spinal cord sections of *Tsc2*^{ff}*FoxD1*$^{GC+}$ mice demonstrate high pS6 (S240/S244) levels in spinal cord neurons (**E**, **F**). (**G–I**) Spinal cord neurons from control mice showed normal, low expression of pS6(S240/S244) (**H**, **I**).

Subsequent studies have shown that this fusion is highly consistent in SFT, with prevalence over 90% in several series (31,32). The fusion involves different exons of *NAB2* and *STAT6*, and the precise fusion site appears to influence clinical behavior of SFT (33), though further study is needed. The fusion event leads to the constitutive location of the fusion protein in the nucleus, as shown by consistent nuclear localization of both proteins by IHC in SFT (30). This occurrence is thought to lead to

constitutive STAT6 signaling. In addition, the Akt/mTOR pathway is reported to be activated in a substantial fraction of SFT/HPC (34). Our observations suggest that mTORC1 is a driver of HPC in mice, while STAT6 is a driver in human HPC, suggesting the possibility that the two genetic events have similar pathway outcomes in pericytes.

Previous studies have noted that renal angiomyolipoma express ANG II type 1 receptors, PDGFR-β, desmin, α-SMA and vascular endothelial growth factor receptor-2 (VEGF receptor 2), suggesting that angiomyolipoma are derived from pericytes (22). Furthermore, serum from TSC patients with angiomyolipoma have increased levels of VEGF-A, VEGF-D, soluble VEGF receptor 2 and collagen type IV (35,36), and VEGFD is also increased in patients with lung lymphangioleiomyomatosis (37). As noted, we found that none of the kidneys or lungs from 8 *Tsc2*^{ff}*FoxD1*$^{GC+}$ mice showed evidence of either of these tumors, despite clear evidence of recombination in kidney pericytes (Fig. 4). Therefore, our data suggest that angiomyolipoma and lymphangioleiomyomatosis do not derive from pericytes. *Foxd1* is reported to be expressed at embryonic days 6–8 (E6-8) during development in the mouse (38,12), and to be expressed in all types of pericytes. Furthermore, we achieved robust recombination in *Tsc2*^{ff}*FoxD1*$^{GC+}$ pericytes leading to development of HPC in multiple organs. Nonetheless, it is possible that a different timing of recombination in pericytes is required to lead to angiomyolipoma and/or lymphangioleiomyomatosis, that pericyte development differs significantly in human and mouse, making it impossible to generate these tumors from pericytes in the mouse, or that the *FoxD1* cre allele is not expressed in all pericytes, missing the pericytes that give rise to these tumors.

Typical renal angiomyolipoma are composed of varying proportions of poorly organized blood vessels, immature SMCs, epithelioid cells and fat cells (21). Previous studies have shown that all components express pericyte markers to some degree, suggesting that all renal angiomyolipoma cells are derived from pericytes (22,23). In our mouse model, it seems that pericytes efficiently give rise to HPCs directly as a consequence of Tsc2 loss. However, it is notable that pericytes are present in all organs, and we have shown in many organs that there is recombination and loss of Tsc2 in pericytes. Nonetheless, we saw HPC development only in selected sites, not in the lung or kidney. There are many possible explanations for this, including different developmental patterns in mouse than in human, and the role of other cell types in tumor development, the microenvironment. Hence, our studies do not exclude the possibility that angiomyolipoma and lymphangioleiomyomatosis derive from pericytes in patients, and further study is required.

Materials and Methods

Mice

Tsc2^{ff} mice were previously generated (25) and were a gift from Elizabeth Henske. The *Foxd1*$^{tm1(GFP/cre)Amc}$ (aka *FoxD1*^{GC}) allele was obtained from the Jackson Laboratory (Stock No: 012463). Mice bearing these alleles were interbred in a mixed strain background to produce *Tsc2*^{ff} *FoxD1*$^{GC+}$ mice, as well as control mice with genotypes *Tsc2*^{fw} *FoxD1*$^{GC+}$ and *Tsc2*^{ff} *FoxD1*$^{GC-}$. The *tdTomato* reporter allele was from Jackson Laboratory (39).

Immunohistochemistry

IHC staining was performed as follows. Tissues were fixed in Bouin's fixative (Poly Scientific R&D Corp, #s129-32OZ) overnight, embedded in paraffin, sectioned, deparaffinized in xylene and rehydrated in an ethanol dilution series. Endogenous peroxidase activity was blocked using 3% H_2O_2. Antigen retrieval was performed by boiling slides in Dako Target Retrieval Solution (Dako, S169984-2) for 7–10 min. Slides were blocked with 5% normal goat serum (Abcam, ab7481) in Phosphate-buffered saline (PBS) with 0.025% Trition-X100 PBST for 1 h at room temperature. Tissues were then interrogated with the following primary antibodies overnight at 4°C: phospho-S6 Ribosomal Protein (Ser240/244) (pS6) (Cell Signaling Technology, #5364S, 1:2000), Vimentin (Cell Signaling Technology, #5741S, 1:200), NG2 (Abcam, ab129051, 1:250), PDGFR-β (Cell Signaling Technology, #4564S, 1:200), CD31 (Abcam, #ab28364, 1:20), Phospho-Histone H3 (Ser10) (Cell Signaling Technology, #9701S, 1:200). Following rinses in 1x PBST, HRP-linked secondary antibodies were incubated at room temperature for 1 h, rinsed with 1x PBST and visualized with AEC (Dako Envision™ + System-HRP (AEC/DAB), #K4009). Slides were counterstained with hematoxylin (Sigma, #H9627) for 1 min then mounted using Fluoromount-G clear liquid mounting medium (SouthernBiotech, #0100-01).

Immunofluorescence

For IF, anti-pS6 (S244/246) was the same as mentioned above for IHC. Anti-vimentin (Santa Cruz Biotechnology, #sc-373717) was used as primary antibody. Slides were incubated using Mouse on Mouse (M.O.M.™) Blocking Reagent (Vector Laboratories, #MKB-2213) for 1 h after 5% normal goat serum blocking. Goat anti-Mouse IgG (H+L) Cross-Adsorbed Secondary Antibody, Alexa Fluor 488 (Thermo Fisher Scientific, #A-11001) and Goat anti-Rabbit IgG (H+L) Cross-Adsorbed Secondary Antibody Alexa Fluor 594 (Cell Signaling Technologies, #A-11012) secondary antibodies were employed (1:500). Vector® TrueVIEW™ Autofluorescence Quenching Kit (Vector Laboratories, #SP-8400) were used to eliminate autofluorescence from parrafin-embedded tissues. Slides were mounted using ProLong Diamond Antifade Mountant with DAPI (Life Technologies, #P36966). IHC and IF slides were viewed using a FSX100 (Olympus) microscope.

Statistical analysis

Means and standard deviations were calculated, and the Wilcoxon rank-sum test was used to compare mouse body weight and lengths. All P-values < 0.05 are considered to be significant.

Supplementary Material

Supplementary Material is available at *HMG* online.

Acknowledgements

National Institutes of Health (NIH) (grant P01 CA120964); The Engles Family Lymphangioleiomyomatosis (LAM)/TS Research Fund.

Conflict of Interest statement. None declared.

References

1. Stout, A.P. and Murray, M.R. (1942) Hemangiopericytoma: a vascular tumor featuring zimmermann's pericytes. *Ann. Surg.*, **116**, 26–33.

2. Tsuneyoshi, M., Daimaru, Y. and Enjoji, M. (1984) Malignant hemangiopericytoma and other sarcomas with hemangiopericytoma-like pattern. *Pathol. Res. Pract.*, **178**, 446–453.
3. Angervall, L., Kindblom, L.G., Nielsen, J.M., Stener, B. and Svendsen, P.L. (1978) Hemangiopericytoma: a clinicopathologic, angiographic and microangiographic study. *Cancer*, **42**, 2412–2427.
4. Enzinger, F.M. and Smith, B.H. (1976) Hemangiopericytoma: an analysis of 106 cases. *Hum. Pathol.*, **7**, 61–82.
5. Pavelic, K., Cabrijan, T.C., Hrascan, R., Vrkljan, M., Lipovac, M., Kapitanovic, S., Gall-Troslj, S.K., Bosnar, M.H., Tomac, A., Grskovic, B.G. *et al.* (1998) Molecular pathology of hemangiopericytomas accompanied by severe hypoglycemia: oncogenes, tumor-suppressor genes and the insulin-like growth factor family. *J. Cancer Res. Clin. Oncol.*, **124**, 307–314.
6. Alen, J.F., Lobato, R.D., Gomez, P.A., Boto, G.R., Lagares, A., Ramos, A. and Ricoy, J.R. (2001) Intracranial hemangiopericytoma: study of 12 cases. *Acta. Neurochir.(Wien)*, **143**, 575–586.
7. Melone, A.G., D'Elia, A., Santoro, F., Salvati, M., Delfini, R., Cantore, G. and Santoro, A. (2014) Intracranial hemangiopericytoma–our experience in 30 years: a series of 43 cases and review of the literature. *World Neurosurg.*, **81**, 556–562.
8. Armulik, A., Genove, G. and Betsholtz, C. (2011) Pericytes: developmental, physiological, and pathological perspectives, problems, and promises. *Dev. Cell.*, **21**, 193–215.
9. Gaengel, K., Genove, G., Armulik, A. and Betsholtz, C. (2009) Endothelial-mural cell signaling in vascular development and angiogenesis. *Arterioscler Thromb Vasc. Biol.*, **29**, 630–638.
10. Stratman, A.N., Malotte, K.M., Mahan, R.D., Davis, M.J. and Davis, G.E. (2009) Pericyte recruitment during vasculogenic tube assembly stimulates endothelial basement membrane matrix formation. *Blood*, **114**, 5091–5101.
11. Diaz-Flores, L., Gutierrez, R., Madrid, J.F., Varela, H., Valladares, F., Acosta, E., Martin-Vasallo, P. and Diaz-Flores, L. Jr. (2009) Pericytes. Morphofunction, interactions and pathology in a quiescent and activated mesenchymal cell niche. *Histol. Histopathol.*, **24**, 909–969.
12. Kramann, R., Schneider, R.K., DiRocco, D.P., Machado, F., Fleig, S., Bondzie, P.A., Henderson, J.M., Ebert, B.L. and Humphreys, B.D. (2015) Perivascular Gli1+ progenitors are key contributors to injury-induced organ fibrosis. *Cell Stem Cell*, **16**, 51–66.
13. Dellavalle, A., Sampaolesi, M., Tonlorenzi, R., Tagliafico, E., Sacchetti, B., Perani, L., Innocenzi, A., Galvez, B.G., Messina, G., Morosetti, R. *et al.* (2007) Pericytes of human skeletal muscle are myogenic precursors distinct from satellite cells. *Nat. Cell Biol.*, **9**, 255–267.
14. Birbrair, A., Zhang, T., Wang, Z.M., Messi, M.L., Enikolopov, G.N., Mintz, A. and Delbono, O. (2013) Skeletal muscle pericyte subtypes differ in their differentiation potential. *Stem Cell Res.*, **10**, 67–84.
15. Crisan, M., Yap, S., Casteilla, L., Chen, C.W., Corselli, M., Park, T.S., Andriolo, G., Sun, B., Zheng, B., Zhang, L. *et al.* (2008) A perivascular origin for mesenchymal stem cells in multiple human organs. *Cell Stem Cell*, **3**, 301–313.
16. Farrington-Rock, C., Crofts, N.J., Doherty, M.J., Ashton, B.A., Griffin-Jones, C. and Canfield, A.E. (2004) Chondrogenic and adipogenic potential of microvascular pericytes. *Circulation*, **110**, 2226–2232.
17. Dibble, C.C., Elis, W., Menon, S., Qin, W., Klekota, J., Asara, J.M., Finan, P.M., Kwiatkowski, D.J., Murphy, L.O. and Manning, B.D. (2012) TBC1D7 is a third subunit of the TSC1-TSC2 complex upstream of mTORC1. *Mol. Cell*, **47**, 535–546.
18. Inoki, K., Corradetti, M.N. and Guan, K.L. (2005) Dysregulation of the TSC-mTOR pathway in human disease. *Nat. Genet*, **37**, 19–24.
19. Guertin, D.A. and Sabatini, D.M. (2007) Defining the role of mTOR in cancer. *Cancer Cell*, **12**, 9–22.
20. Laplante, M. and Sabatini, D.M. (2012) mTOR signaling in growth control and disease. *Cell*, **149**, 274–293.
21. Karbowniczek, M., Yu, J. and Henske, E.P. (2003) Renal angiomyolipomas from patients with sporadic lymphangiomyomatosis contain both neoplastic and non-neoplastic vascular structures. *Am. J. Pathol.*, **162**, 491–500.
22. Shen, J., Shrestha, S., Yen, Y.H., Scott, M.A., Asatrian, G., Barnhill, R., Lugassy, C., Soo, C., Ting, K., Peault, B. *et al.* (2015) Pericyte antigens in angiomyolipoma and PEComa family tumors. *Med. Oncol*, **32**, 210.
23. Siroky, B.J., Yin, H., Dixon, B.P., Reichert, R.J., Hellmann, A.R., Ramkumar, T., Tsuchihashi, Z., Bunni, M., Dillon, J. and Bell, P.D. (2014) Evidence for pericyte origin of TSC-associated renal angiomyolipomas and implications for angiotensin receptor inhibition therapy. *Am. J. Physiol. Renal. Physiol.*, **307**, F560–F570.
24. Humphreys, B.D., Lin, S.L., Kobayashi, A., Hudson, T.E., Nowlin, B.T., Bonventre, J.V., Valerius, M.T., McMahon, A.P. and Duffield, J.S. (2010) Fate tracing reveals the pericyte and not epithelial origin of myofibroblasts in kidney fibrosis. *Am. J. Pathol.*, **176**, 85–97.
25. Hernandez, O., Way, S., McKenna, J. III and Gambello, M.J. (2007) Generation of a conditional disruption of the Tsc2 gene. *Genesis*, **45**, 101–106.
26. Wu, H., Wu, Z., Li, P., Cong, Q., Chen, R., Xu, W., Biswas, S., Liu, H., Xia, X., Li, S. *et al.* (2017) Bone size and quality regulation: concerted actions of mTOR in mesenchymal stromal cells and steoclasts. *Stem Cell Reports*, **8**, 1600–1616.
27. Meikle, L., Talos, D.M., Onda, H., Pollizzi, K., Rotenberg, A., Sahin, M., Jensen, F.E. and Kwiatkowski, D.J. (2007) A mouse model of tuberous sclerosis: neuronal loss of Tsc1 causes dysplastic and ectopic neurons, reduced myelination, seizure activity, and limited survival. *J. Neurosci.*, **27**, 5546–5558.
28. Yuan, E., Tsai, P.T., Greene-Colozzi, E., Sahin, M., Kwiatkowski, D.J. and Malinowska, I.A. (2012) Graded loss of tuberin in an allelic series of brain models of TSC correlates with survival, and biochemical, histological and behavioral features. *Hum. Mol. Genet.*, **21**, 4286–4300.
29. Fletcher, C.D., Hogendoorn, P., Mertens, F. and Bridge, J. (2013) *WHO Classifica-tion of Tumours of Soft Tissue and Bone*, 4th edn. IARC Press, Lyon, France.
30. Schweizer, L., Koelsche, C., Sahm, F., Piro, R.M., Capper, D., Reuss, D.E., Pusch, S., Habel, A., Meyer, J., Göck, T. *et al.* (2013) Meningeal hemangiopericytoma and solitary fibrous tumors carry the NAB2-STAT6 fusion and can be diagnosed by nuclear expression of STAT6 protein. *Acta. Neuropathologica.*, **125**, 651–658.
31. Chmielecki, J., Crago, A.M., Rosenberg, M., O'Connor, R., Walker, S.R., Ambrogio, L., Auclair, D., McKenna, A., Heinrich, M.C., Frank, D.A. *et al.* (2013) Whole-exome sequencing identifies a recurrent NAB2-STAT6 fusion in solitary fibrous tumors. *Nat. Genet.*, **45**, 131–132.
32. Robinson, D.R., Wu, Y.M., Kalyana-Sundaram, S., Cao, X., Lonigro, R.J., Sung, Y.S., Chen, C.L., Zhang, L., Wang, R., Su, F. *et al.* (2013) Identification of recurrent NAB2-STAT6 gene fusions in solitary fibrous tumor by integrative sequencing. *Nat. Genet.*, **45**, 180–185.

33. Barthelmess, S., Geddert, H., Boltze, C., Moskalev, E.A., Bieg, M., Sirbu, H., Brors, B., Wiemann, S., Hartmann, A., Agaimy, A. *et al.* (2014) Solitary fibrous tumors/hemangiopericytomas with different variants of the NAB2-STAT6 gene fusion are characterized by specific histomorphology and distinct clinicopathological features. *Am. J. Pathol.*, **184**, 1209–1218.
34. Yamada, Y., Kohashi, K., Fushimi, F., Takahashi, Y., Setsu, N., Endo, M., Yamamoto, H., Tokunaga, S., Iwamoto, Y. and Oda, Y. (2014) Activation of the Akt-mTOR pathway and receptor tyrosine kinase in patients with solitary fibrous tumors. *Cancer*, **120**, 864–876.
35. Budde, K., Zonnenberg, B.A., Frost, M., Cheung, W., Urva, S., Brechenmacher, T., Stein, K., Chen, D., Kingswood, J.C. and Bissler, J.J. (2016) Pharmacokinetics and pharmacodynamics of everolimus in patients with renal angiomyolipoma and tuberous sclerosis complex or lymphangioleiomyomatosis. *Br. J. Clin. Pharmacol.*, **81**, 958–970.
36. Dodd, K.M., Yang, J., Shen, M.H., Sampson, J.R. and Tee, A.R. (2015) mTORC1 drives HIF-1α and VEGF-A signalling via multiple mechanisms involving 4E-BP1, S6K1 and STAT3. *Oncogene*, **34**, 2239–2250.
37. Xu, K.F., Zhang, P., Tian, X., Ma, A., Li, X., Zhou, J., Zeng, N., Gui, Y.S., Guo, Z., Feng, R. *et al.* (2013) The role of vascular endothelial growth factor-D in diagnosis of lymphangioleiomyomatosis (LAM). *Respir. Med.*, **107**, 263–268.
38. Koga, M., Matsuda, M., Kawamura, T., Sogo, T., Shigeno, A., Nishida, E. and Ebisuya, M. (2014) Foxd1 is a mediator and indicator of the cell reprogramming process. *Nat. Commun.*, **5**, 3197.
39. Madisen, L., Zwingman, T.A., Sunkin, S.M., Oh, S.W., Zariwala, H.A., Gu, H., Ng, L.L., Palmiter, R.D., Hawrylycz, M.J., Jones, A.R. *et al.* (2010) A robust and high-throughput Cre reporting and characterization system for the whole mouse brain. *Nat. Neurosci.*, **13**, 133–140.